Letters in Applied NanoBioScience
Open-Access Journal (ISSN: 2284-6808)

Article
Volume 15, Issue 2, 2026, 63
https://doi.org/10.33263/LIANBS152.063

Investigating the Optical, Morphological, and Structural Properties of Ceria (CeO/CeO_2) Nanoparticles from *Withania Somnifera* for Bio-Application Study

Geeta Nayak [1], Santosh Mallikarjun Bhavi [2], Arati Sanadi [1], Shruti Guttedar [1], Shivaleela Biradar [1], Akshata Choudhari Padti [2], Bothe Thokchom [2], Sapam Riches Singh [2], Ramesh Babu Yarajarla [2], Babu R. Lamani [1,*]

[1] Laboratory of Natural Compound and Drug Discovery, Department of P. G. Studies and Research in Bioinformatics and Biotechnology, Vijayapura, Karnataka, India; geetanayak360@gmail.com (G.N.); aratisanadi2001@gmail.com (A.S.); shrutiguttedar568@gmail.com (S.G.); shivaleelabiradar4@gmail.com (S.B.); babu@kswu.ac.in (B.R.L.);
[2] Drosophila and Nanoscience Research Laboratory, Department of Applied Genetics, Karnatak University, Dharwad, Karnataka – 580003, India; santosh.b@kud.ac.in (S.M.B.); akshatapadti@kud.ac.in (A.C.P.); bothe@kud.ac.in (ORCiD:) (B.T.); sapam@kud.ac.in (S.R.S.); rameshy@kud.ac.in (R.B.Y.);
* Correspondence: babu@kswu.ac.in (B.R.L.);

Received: 21.03.2025; Accepted: 23.08.2025; Published: 30.06.2026

Abstract: This study demonstrates the green synthesis of cerium oxide nanoparticles (Ceria-NPs) using *Withania somnifera* leaf extract (WS-Ceria-NPs), providing an eco-friendly and biocompatible alternative to conventional physicochemical routes. The phytochemicals in *W. somnifera* act as natural reducing and stabilizing agents, imparting additional biofunctional properties to the nanoparticles. The synthesized WS-Ceria-NPs were extensively characterized by UV-Vis spectroscopy, FTIR, SEM, EDX, XRD, zeta potential analysis, and HRTEM, confirming their crystalline structure, stability, and average size of 20–35 nm. A key innovation of this work is the observation of dual band gap energies (3.8 eV and 2.1 eV), arising from oxygen vacancies and Ce^{3+}/Ce^{4+} redox cycling, which enhance their catalytic and biomedical potential. Biocompatibility studies revealed significant antibacterial activity against *Escherichia coli* (inhibition zone ~18 mm), strong antioxidant capacity (82% DPPH scavenging at 100 µg mL^{-1}, surpassing ascorbic acid), and potent anti-inflammatory effects (74% inhibition of protein denaturation). Moreover, the nanoparticles effectively reduced nitric oxide levels by ~45% in LPS-treated colon cancer pancreatic cells, demonstrating their ability to modulate oxidative stress and inflammation. These findings underscore the innovation and importance of integrating medicinal plant extracts into nanomaterial synthesis to generate multifunctional, stable, and clinically relevant nanomaterials for antimicrobial, antioxidant, and anti-inflammatory biomedical applications.

Keywords: *Withania somnifera*; ceria nanoparticles; green synthesis; characterization; biomedical applications.

1. Introduction

The advent of nanotechnology has introduced the study of nanoparticulate systems in a new era of innovation in biomedical and environmental sciences [1,2]. Through its lens, the synthesis and application of nanoparticles with tailored physicochemical characteristics have transformed the field of scientific exploration [3,4]. Silver [5–7], gold [8], carbon dots [9,10], zinc oxide [11,12], and titanium dioxide [13], copper oxide [14] nanoparticles, which have been extensively studied for their antimicrobial, catalytic, and other applications, are some of the glaring examples [15–18]. Among metal oxide nanoparticles, cerium oxide nanoparticles

(CeO_2NPs) have gained significant attention due to their distinctive redox properties, biocompatibility, and diverse biomedical applications [19]. The ability of CeO_2NPs to transition between Ce^{4+} and Ce^{3+} oxidation states allows them to function as effective antioxidants and radical scavengers. Studies have demonstrated the efficacy of CeO_2NPs in mitigating reactive oxygen species (ROS)-induced cellular damage [20]. In addition to their redox capabilities, CeO_2NPs synthesized using plant-based methods have shown improved biocompatibility and stability compared to those synthesized through conventional physicochemical routes. With the growing demand for sustainable nanomaterials, plant-mediated synthesis has emerged as a viable alternative, which reduces the need for hazardous chemicals and high-energy inputs commonly associated with traditional synthesis methods [21,22]. Despite these advances, challenges remain in achieving eco-friendly, scalable, and multifunctional nanoparticle synthesis that can bridge the gap between material design and biomedical applications [23,24].

Nanoparticles can be synthesized via physical, chemical, or biological routes. While physical and chemical methods such as sol–gel, co-precipitation, and hydrothermal techniques are widely used, they often require high energy and hazardous reagents [25,26]. Biological or 'green' synthesis, on the other hand, employs plant extracts, microorganisms, or biomolecules as reducing and stabilizing agents, offering eco-friendly and biocompatible alternatives [27]. Plant-mediated approaches are particularly attractive, as phytochemicals play a dual role in reducing metal ions and stabilizing nanoparticles, aligning with the current emphasis on sustainable nanomaterials for biomedical applications [28].

Withania somnifera has been extensively used in traditional medicine for its adaptogenic, antioxidant, anti-inflammatory, and rejuvenating properties. Also commonly known as Ashwagandha, it has played a vital role in Ayurveda and other ethnomedicinal systems, while addressing conditions such as stress, arthritis, and neurodegenerative disorders [29]. The phytochemicals present in its leaf extract, such as flavonoids, alkaloids, and tannins, contribute to its therapeutic potential and enhance the stability of nanoparticles synthesized using green chemistry approaches [30]. Although other plants have been used for the biosynthesis of CeO_2 nanoparticles, reports on *W. somnifera*-mediated synthesis remain scarce. Its unique phytochemicals not only stabilize nanoparticles but may also impart additional therapeutic properties, a feature underexplored in previous studies. Notably, other species within the Withania genus, such as Withania coagulans, have also been reported for nanoparticle synthesis, in which their phytochemicals facilitate antifungal, antimicrobial, and photocatalytic applications [31,32]. These studies highlight the potential of the genus Withania across green nanotechnology, whereas our work focuses specifically on the biomedical applications of *W. somnifera*-derived ceria nanoparticles. The role of plant-derived CeO_2NPs in augmenting biological functionalities by facilitating better dispersibility and biocompatibility has been studied [33]. The use of *W. somnifera* extract for nanoparticle synthesis offers additional benefits, including reduced cytotoxicity and the incorporation of bioactive compounds that can further enhance the therapeutic properties of CeO_2NPs [19].

The rise of antibiotic-resistant bacterial strains calls for the exploration of alternative antimicrobial agents [34]. Nanoparticles, including CeO_2NPs, have demonstrated bactericidal properties through mechanisms such as oxidative stress induction and membrane disruption [35]. The evaluation of antioxidant activity is particularly important, as oxidative stress is implicated in the pathophysiology of several chronic diseases, including neurodegenerative disorders [36], diabetes [37], and cardiovascular conditions [38]. CeO_2NPs have been reported

to mimic superoxide dismutase (SOD) and catalase-like activity, aiding in ROS neutralization [39]. Moreover, inflammation is a key factor in the progression of various diseases, including rheumatoid arthritis, inflammatory bowel disease, and cancer, in which chronic inflammatory responses contribute to tissue damage and disease progression [40]. Since prolonged inflammation is linked to autoimmune disorders and cancer progression, nanoparticles capable of modulating inflammatory responses may also have significant therapeutic implications [41]. However, most earlier works focused on either structural characterization or a single type of bioactivity, whereas this study integrates comprehensive characterization with multiple biological assays to demonstrate the multifunctionality of WS-Ceria-NPs.

The innovation of this study lies in utilizing *W. somnifera* leaf extract to produce stable CeO_2 nanoparticles with unique dual band gap energies and multifunctional bioactivity. This eco-friendly approach highlights the importance of integrating medicinal plants into green nanotechnology to generate nanomaterials suitable for antimicrobial therapy, oxidative stress management, and inflammation control. The present work provides a comprehensive synthesis-to-application investigation of WS-Ceria-NPs, combining detailed physicochemical characterization with antibacterial, antioxidant, and anti-inflammatory evaluations to demonstrate their biomedical potential.

2. Materials and Methods

This section describes the materials, synthesis procedure, characterization techniques, and biological assays used to investigate WS-Ceria-NPs.

2.1. Materials and reagents.

The following chemicals and biological materials were used in this study: Cerium nitrate hexahydrate ($Ce(NO_3)_3 \cdot 6H_2O$, ≥99% purity) (1 mM) (Sigma-Aldrich, CAS No: 10294-41-4, Product Code: 238538), Sodium hydroxide (NaOH, analytical grade) (0.03 M) (Merck, CAS No: 1310-73-2), Methanol (SRL, CAS No: 67-56-1), DPPH (2,2-diphenyl-1-picrylhydrazyl, ≥95%) (Sigma-Aldrich, CAS No: 1898-66-4), Phosphate-buffered saline (PBS, pH 7.4) (Thermo Fisher Scientific, Product Code: 10010023), Bovine Serum Albumin (BSA, ≥98%) (Sigma-Aldrich, CAS No: 9048-46-8), Ciprofloxacin (HiMedia, CAS No: 85721-33-1), Lipopolysaccharide (LPS, from *E. coli* O55:B5, ≥99%) (Sigma-Aldrich, CAS No: 93572-42-0), Griess Reagent Kit (Thermo Fisher Scientific, Product Code: G7921), *Escherichia coli* (*E. coli*, ATCC 25922), and Colon Cancer Pancreatic Cells (National Centre for Cell Science, NCCS Pune, India, Product Code: NCCS-5002 for PANC-1). *W. somnifera* leaves were collected from the botanical garden of KSAWU Vijayapura, which was identified and authenticated by Dr. Shivanand S. Bhat, Taxonomist, Smt. Indira Gandhi Government First Grade Women's College, Sagar, Karnataka, India (Specimen Acc. No: IGGFWC/Sol-050). All chemicals were of analytical grade and used without further purification.

2.2. Plant extract preparation and synthesis of ceria nanoparticles.

The synthesis of plant extract and nanoparticles was carried out following the method of Khaoula Hkiri *et al*., with slight modifications [42]. *W. somnifera* leaves were washed thoroughly with running tap water and then with deionized water. The leaves were allowed to dry at room temperature until all moisture evaporated, and then ground into a coarse powder using an electric blender. 10 g of the dried leaf powder was added to 100 mL of deionized water

and mixed thoroughly. The mixture was heated for 10 min at 60–70°C, and the extract was filtered through Whatman filter paper No. 1. To the filtrate, 3.72 g of cerium nitrate hexahydrate (1 mM) was added and mixed. The resulting solution was stirred on a magnetic stirrer at 60°C for 3–5 h under constant stirring in a closed flask. A sterile burette was set up with 0.03 M sodium hydroxide solution and used to titrate the mixture dropwise until precipitation was observed, adjusting the final pH to ~9.0–9.5 to facilitate nanoparticle formation. The precipitate was allowed to settle, centrifuged at 10,000 rpm for 15 min, and washed three times with deionized water and ethanol to remove residual impurities. The washed material was transferred to a crucible and dried in a muffle furnace at 220°C for 2 h to obtain a grey-colored CeO_2 nanoparticle powder. The dried nanoparticles were collected, finely ground, and stored in airtight containers at room temperature until further use.

2.3. Characterizations.

Characterization of nanoceria involves a range of analytical techniques to assess its size, morphology, composition, structure, stability, and other physicochemical properties. The synthesized nanoceria, typically procured in powder form, was characterized using UV-Vis spectrophotometry, FTIR, SEM, EDS, XRD, zeta potential analysis, and HRTEM. UV-Visible spectrophotometry is a simple and prominent technique that measures absorbance in the range of 200–800 nm, with a scan speed of 400 nm/min and a resolution of 1 nm, influenced by factors like extrinsic vibrations and contaminants. The absorbance of nanoceria in UV is attributed to the charge alteration between O^{2-} and Ce^{4+} ions, and the characterization involves recording absorbance at various wavelengths. For this study, the JASCO V-670 UV-Vis-NIR Spectrophotometer was used. FTIR provides molecular fingerprints of nanoceria, identifies unknown materials, determines functional groups, and checks consistency. The analysis was conducted in the 4000–600 cm^{-1} range with a resolution of 4 cm^{-1}, averaging 32 scans per sample using a PerkinElmer Spectrum instrument, with IR radiation absorbed and transmitted by the sample. SEM examines morphology, texture, and pore size by interacting with the sample surface, scattering electrons that are detected to form images. Nanoceria powder was ultrasonicated with a volatile solvent, such as alcohol or acetone, and a droplet of the suspension was placed on a stub substrate, dried, and analyzed using the JEOL JSM-IT500 instrument at an accelerating voltage of 15 kV. EDS, integrated with SEM, enables chemical composition analysis by detecting characteristic X-rays emitted when a core-shell electron is ejected by an electron beam. XRD is used to determine crystalline grain size, phase composition, and crystal structure, analyzing diffraction patterns in the 2θ range of 10°–90°, with a step size of 0.02° and a scan rate of 2°/min, using Cu Kα radiation (λ = 1.5406 Å). Zeta Potential Analysis, measured using the HORIBA SZ-100, evaluates the surface charge of nanoparticles under an electric field by measuring electrophoretic mobility via laser Doppler velocimetry and applying the Henry equation. Samples were prepared by dispersing 1 mg mL^{-1} of nanoparticles in deionized water, ultrasonicated for 15 min, and measured at 25°C with data averaged over three runs. HRTEM provides high-resolution imaging to measure particle size, size distribution, and morphology at the atomic scale. The analysis was conducted using the Jeol/JEM 2100 HRTEM, equipped with a 200 kV LaB6 electron gun, a point resolution of 0.23 nm, a lattice resolution of 0.14 nm, and SAED capabilities. Nanoceria samples for HRTEM were prepared by dispersing the powder in ethanol, ultrasonically for 20 min, then placing a small droplet on a grid, drying under vacuum, and imaging at various locations to obtain representative data.

2.4. Biocompatibility studies.

The biological potential of WS-Ceria-NPs was assessed through antibacterial, antioxidant, anti-inflammatory, and nitric oxide inhibition assays, as outlined in the following subsections.

2.4.1. Antibacterial activity.

The antibacterial potential of freshly prepared WS-Ceria-NPs was evaluated against *Escherichia coli*, a gram-negative bacterium, in comparison to Ciprofloxacin, an antibiotic effective against *E. coli*. Nutrient agar media was prepared by autoclaving and cooling it to a warm temperature, then pouring it into Petri plates, where it solidified for 30 min. Freshly prepared bacterial broth culture inoculum of *E. coli* was spread uniformly on the agar plates [43]. Wells were created using a syringe punch of specified diameter, and 100 µg of WS-Ceria-NPs solution was added to each well. A Ciprofloxacin antibiotic disc was placed on the agar plate as the positive control. The plates were incubated at 37°C for 24 h, and the bacterial growth inhibition zones around the well and the antibiotic disc were observed and measured.

2.4.2. Minimum inhibitory concentration (MIC) determination.

The MIC of WS-Ceria-NPs was determined using the standard broth microdilution method according to CLSI guidelines (M07-A8). Two-fold serial dilutions of the nanoparticles were prepared in Mueller-Hinton broth to obtain final concentrations ranging from 500 to 31.25 µg mL^{-1}. The bacterial inoculum was adjusted to approximately 5×10^5 CFU mL^{-1} and added to each dilution. A growth control containing inoculated broth without nanoparticles was included. All tubes were incubated at 37°C for 24 h, and the MIC was defined as the lowest nanoparticle concentration at which no visible bacterial growth (turbidity) was observed. Turbidity was assessed visually before and after incubation to confirm the MIC value.

2.4.3. Free radical scavenging assay.

The antioxidant activity was assessed using the DPPH radical scavenging method, a popular, quick, and affordable approach based on the ability of antioxidants to scavenge free radicals. The antioxidant activity of nanoceria was compared to that of standard ascorbic acid. Samples of 50 µg mL^{-1}, 100 µg mL^{-1}, 150 µg mL^{-1}, 200 µg mL^{-1}, and 250 µg mL^{-1} concentrations of nanoceria, as well as ascorbic acid at concentrations from 50 µg mL^{-1} to 250 µg mL^{-1}, were prepared and conjugated with 5 µg of DPPH in 50 mL of methanol. The mixture was vigorously vortexed and incubated in the dark for 30 min. After incubation, the solution was thoroughly mixed, and the optical density was measured at 517 nm. As a control, 1 mL of DPPH solution was used with various concentrations of distilled water to account for any interference. The DPPH radical scavenging activity (%) was calculated using the following formula:

$$\text{DPPH Scavenging Effect (\%)} = \frac{A_0 - A_1}{A_0} \times 100 \qquad (1)$$

Where: A_0 is the absorbance of the control, and A_1 is the absorbance of the sample with DPPH.

2.4.4. Anti-inflammatory activity of ceria nanoparticles.

The anti-inflammatory activity of WS-Ceria-NPs was evaluated using the protein denaturation method, where the inhibition of albumin denaturation serves as a marker. The anti-inflammatory potential of nanoceria synthesized from *W. somnifera* was compared with the standard drug dexamethasone. Samples with concentrations of 50 µg mL^{-1}, 100 µg mL^{-1}, 150 µg mL^{-1}, 200 µg mL^{-1}, and 250 µg mL^{-1} were prepared. For each sample, 1 mL of PBS and 4 µL of BSA were added. Similarly, varying concentrations of dexamethasone (50 µg mL^{-1} to 250 µg mL^{-1}) were prepared using the same procedure for comparison. The samples were incubated at 70°C for 20 min and then allowed to cool to room temperature for 15 min to induce protein denaturation. The absorbance of the solutions was measured at 660 nm, and the percentage inhibition of protein denaturation was calculated using the following formula:

$$\text{Protein Denaturation Inhibition (\%)} = \frac{A_{control} - A_{sample}}{A_{control}} \times 100 \qquad (2)$$

Where $A_{control}$ is the absorbance of the control (BSA with PBS only), A_{sample} is the absorbance of the sample containing nanoceria or dexamethasone.

2.4.5. Nox assay.

Colon cancer pancreatic cells were seeded into a 6-well polystyrene plate, with 700 µL of cell suspension added to each well, and incubated at 37°C for 24 h to allow complete adhesion. A stock solution of nanoceria was prepared by dissolving 10 mg of nanoceria in 1 mL of deionized water. The cells were treated as follows: Well 1 served as a control; Well 2 received 4 µL of lipopolysaccharide (LPS); Well 3 received LPS (4 µL) along with the nanoceria sample; and Wells 4, 5, and 6 received 20 µL, 40 µL, and 60 µL of the nanoceria sample, respectively. The plate was further incubated for 24 h at 37°C in a CO_2 incubator. After incubation, the supernatant from each well was carefully pipetted into sterile tubes, and an equal volume of Griess reagent was added. The tubes were incubated at room temperature for 10 min, and the absorbance was measured at 540 nm to determine the nitric oxide levels, reflecting the effect of nanoceria on NOX activity.

2.4.6. Statistical analysis.

All experimental data were analyzed using GraphPad Prism 10 (GraphPad Software, USA). One-way analysis of variance (ANOVA) was performed to compare multiple groups, followed by Tukey's post hoc test for pairwise comparisons. Two-way ANOVA was conducted to assess the interaction between independent variables, with Sidak's post hoc test applied for multiple comparisons. A p-value < 0.05 was considered statistically significant. Data are presented as mean ± standard deviation (SD).

3. Results and Discussion

The synthesized WS-Ceria-NPs were evaluated for their structural, morphological, and biological properties, and the findings are presented in the following subsections.

3.1. Ceria nanoparticle synthesis.

Ceria-NPs were successfully synthesized using a green method. A total of 1.5 g of grey-colored Ceria-NPs was obtained from 10 g of *W. somnifera* leaf extract. Cerium nitrate

hexahydrate served as the precursor, and sodium hydroxide was used to facilitate precipitation and adjust the pH. This green synthesis approach highlights the dual role of plant extracts as reducing and stabilizing agents, ensuring an eco-friendly and efficient process. The successful formation of CeO_2 nanoparticles was further confirmed by subsequent spectroscopic and microscopic characterization techniques, as described in the following sections. The synthesis mechanism has been illustrated in Figure 1, depicting the stepwise transformation from cerium precursor to CeO/CeO_2 nanoparticles.

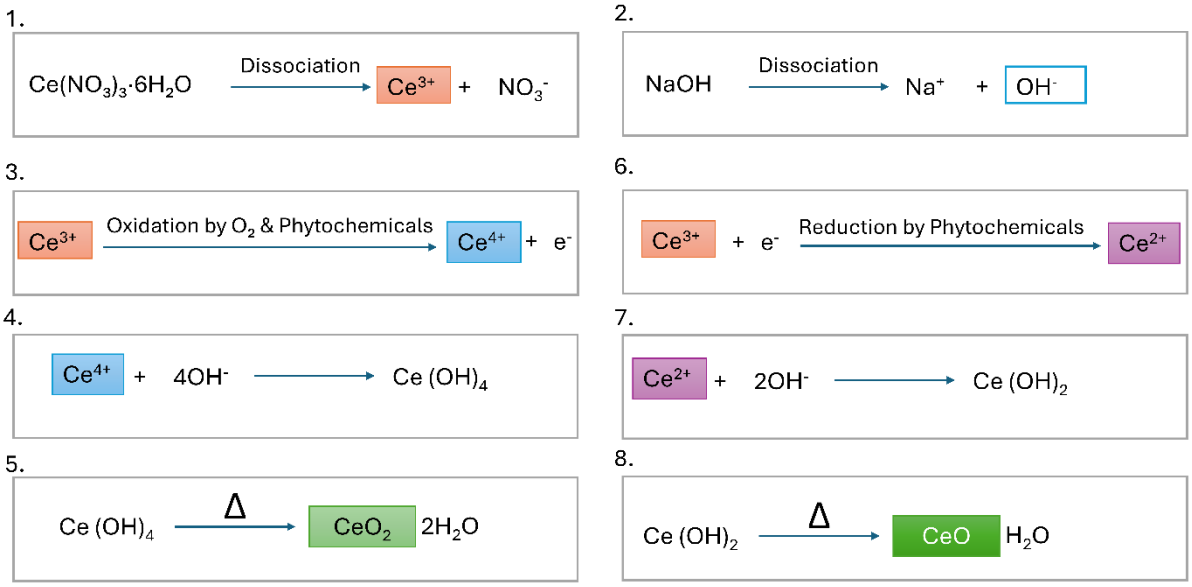

Figure 1. The figure outlines the green synthesis of CeO_2 and CeO nanoparticles from cerium nitrate hexahydrate ($Ce(NO_3)_3·6H_2O$) using *W. somnifera* leaf extract and NaOH. The possible mechanism involves: **(1)** dissociation of $Ce(NO_3)_3·6H_2O$ into Ce^{3+} and NO_3^-; **(2)** dissociation of NaOH into Na^+ and OH^-; **(3)** oxidation of Ce^{3+} by O_2 and phytochemicals to form Ce^{4+}; **(4)** reaction of Ce^{4+} with OH^- to form $Ce(OH)_4$; **(5)** dehydration of $Ce(OH)_4$ to form CeO_2 nanoparticles; **(6)** reduction of Ce^{3+} by phytochemicals to form Ce^{2+}; **(7)** reaction of Ce^{2+} with OH^- to form $Ce(OH)_2$; **(8)** decomposition of $Ce(OH)_2$ to form CeO nanoparticles.

3.2. UV-Vis spectrum analysis and band gap analysis.

The UV-Vis absorption spectrum of WS-Ceria-NPs exhibited two distinct peaks at 256 nm and 363 nm, confirming the presence of both Ce^{3+} and Ce^{4+} oxidation states (Figure 2a). The absorption peak at 279 nm corresponds to cerium(III) (Ce^{3+}), while the peak at 371 nm is associated with cerium(IV) (Ce^{4+}) [44]. This dual absorbance pattern aligns with previous reports indicating that cerium species exhibit characteristic spectrophotometric peaks in the 230–260 nm range for Ce^{3+} and 300–400 nm range for Ce^{4+} [45].

For comparison, Chinnaiah K *et al*. reported that the UV–Vis spectrum of *W. somnifera* leaf extract exhibits two absorption maxima at 348 nm and 377 nm. These peaks are attributed to n-π^* and π-π^* transitions of tyrosine, tryptophan, and phenylalanine residues present in proteins within the extract [46]. In the present study, the absorption peaks of WS-Ceria-NPs at 256 nm and 363 nm differ from those of the plant extract, confirming the successful formation of cerium nanoparticles and highlighting the role of phytochemicals in reducing and capping the nanoparticles.

The energy band gap (E_g) of WS-Ceria-NPs, estimated using Tauc's plot, revealed two distinct band gap values: 3.8 eV and 2.1 eV. The higher band gap (3.8 eV) corresponds to the intrinsic electronic structure of bulk CeO_2, reflecting its insulating nature (Figure 2b). Conversely, the lower band gap (2.1 eV) suggests the presence of oxygen vacancies, surface

defects, and Ce^{3+} states, which introduce mid-gap energy levels, facilitating sub-bandgap electronic transitions [47]. The reduced band gap is characteristic of defect-rich Ceria-NPs, which exhibit enhanced redox cycling (Ce^{3+}/Ce^{4+}), ROS scavenging ability, and enzyme-mimetic catalytic properties.

A previous study reported that mesoporous ceria (MC) exhibits a band gap of 2.8–3.2 eV, making it effective for photocatalytic applications, including contaminant degradation, air purification, water splitting, and gas storage. The smaller crystal size of MC enhances light scattering in a hydrated medium, reducing visible light penetration and improving photocatalytic efficiency [48]. Compared to MC, the lower band gap of WS-Ceria-NPs (2.1 eV) suggests a higher density of oxygen vacancies, which may further enhance photoactivity, oxidative stress modulation, and catalytic efficiency in biomedical and environmental applications.

The coexistence of Ce^{3+} and Ce^{4+} oxidation states underscores the redox-active nature of WS-Ceria-NPs, making them highly functional in antioxidant, antibacterial, and anti-inflammatory applications. The ability of CeO_2 to shuttle between oxidation states is critical for its biomedical and environmental potential, particularly in oxidative stress modulation and catalytic degradation reactions. The dual-band-gap nature of WS-Ceria-NPs highlights their unique electronic properties, confirming their successful synthesis and stability and suggesting promising applications in nanomedicine and catalysis.

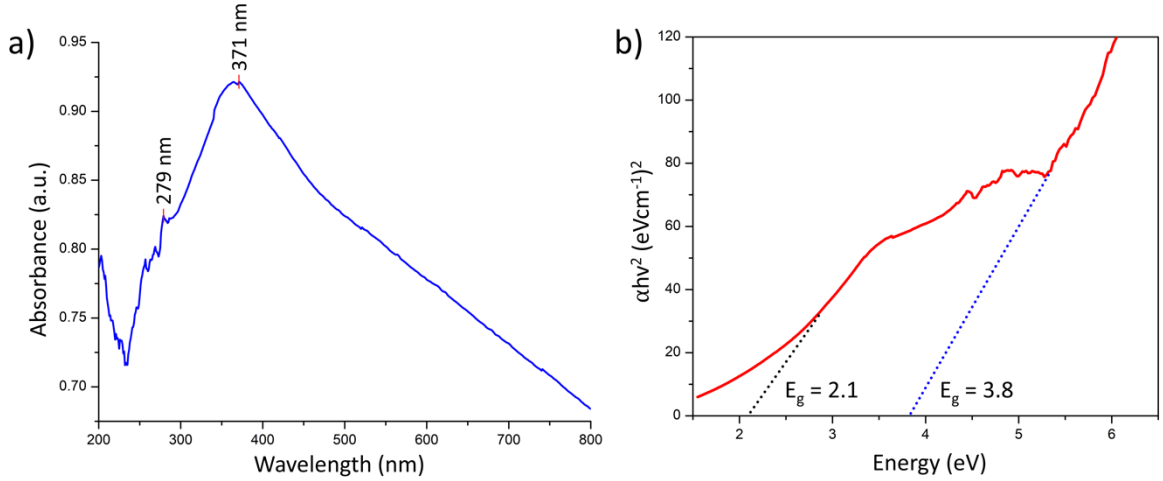

Figure 2. UV-Vis absorption spectrum and Tauc plot of WS-Ceria-NPs. **(a)** UV-Vis spectrum showing absorption peaks at 256 nm and 363 nm, corresponding to Ce^{3+} and Ce^{4+} oxidation states, confirming the redox-active nature of the nanoparticles; **(b)** Tauc plot used for band gap estimation, indicating two distinct band gaps of 3.8 eV and 2.1 eV, associated with bulk CeO_2 and defect-induced electronic transitions, respectively.

3.3. FTIR analysis.

The FTIR spectra of green-synthesized Ceria-NPs were recorded in the range of 4000–600 cm^{-1} to identify the functional groups and confirm nanoparticle formation (Figure 3c). The spectral data are shown in Figure 3. A broad peak at 3946 cm^{-1} is attributed to the stretching vibration of hydroxyl (-OH) groups, which may arise from adsorbed water or hydroxyl functional groups on the nanoparticle surface. A second intense peak at 3777 cm^{-1} further confirms the presence of O-H groups, likely contributed by the phytochemicals in the plant extract used for synthesis. These peaks fall within the typical range for hydroxyl (-OH) stretching vibrations as reported by Fengwei *et al*. [49]. The peak at 2881 cm^{-1} corresponds to C-H stretching vibrations, indicating the presence of residual surfactant or organic compounds from the plant extract. The absorption band at 1374 cm^{-1} is attributed to the bending vibrations

of carbonyl (C=O) groups, likely from carboxylates or ketones in the phytochemicals. In the fingerprint region, several peaks were observed. The peaks at 985 cm^{-1} and 1120 cm^{-1} are associated with C-O stretching vibrations, while the peak at 698 cm^{-1} corresponds to C-H bending. The peak at 637 cm^{-1} corresponds to O-Ce-O stretching, confirming the successful synthesis of Ceria-NPs. This fingerprint peak nearly aligns with the study by Tumkur *et al*., and Subathra *et al*. [50,51]. The observed functional groups, apart from Ce-O and O-Ce-O, arise from the phytochemicals present in the plant extract, which act as capping and stabilizing agents during the synthesis. These include hydroxyl, carbonyl, and carboxyl groups that enhance nanoparticle stability and prevent aggregation. The FTIR analysis thus confirms the formation of Ceria-NPs and highlights the role of plant-derived phytochemicals in functionalizing the nanoparticles.

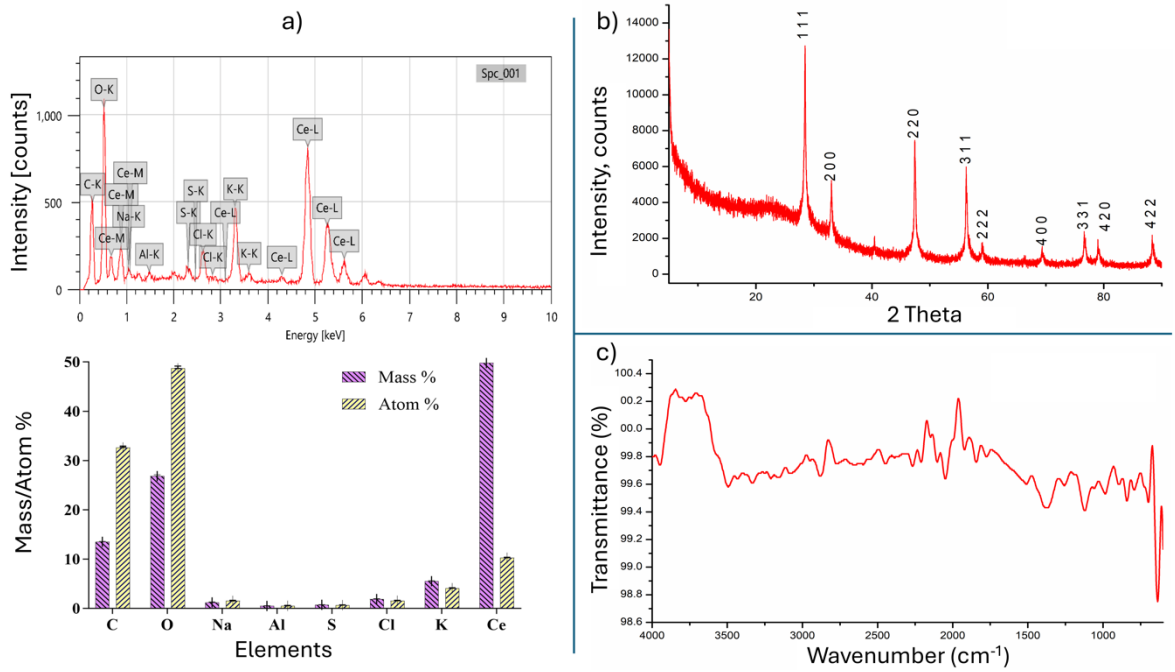

Figure 3. EDX, XRD, and FTIR analysis of WS-Ceria-NPs. **(a)** EDX spectrum confirming the elemental composition of cerium (Ce) and oxygen (O) as primary components, with minor traces of other elements from the plant extract; **(b)** XRD pattern showing characteristic diffraction peaks corresponding to the cubic fluorite structure of CeO_2, confirming crystallinity and nanoscale dimensions; **(c)** FTIR spectrum identifying functional groups involved in nanoparticle stabilization, with peaks corresponding to O-H, C-H, C=O, and Ce-O vibrations, highlighting the role of phytochemicals in nanoparticle synthesis and surface modification.

3.4. SEM analysis.

The WS-Ceria-NPs were subjected to SEM analysis (Figure 4a-d). SEM analysis provided detailed insights into the morphology and size of the nanoparticles. The nanoparticles appeared segregated and exhibited a highly porous and irregular surface, a characteristic also reported in the study by Nor Monica and Aishah [52]. At lower magnifications, the overall distribution and aggregation pattern of the nanoparticles are visible, while higher magnifications reveal finer surface details and the nanoscale texture of the particles. The porous structure, which increases the surface area, is advantageous for applications such as catalysis and drug delivery, enhancing the reactivity and functionality of the nanoparticles [53]. These structural features underscore the effectiveness of the green synthesis method in producing nanoparticles with desirable characteristics. Further morphological and structural details were examined through TEM analysis.

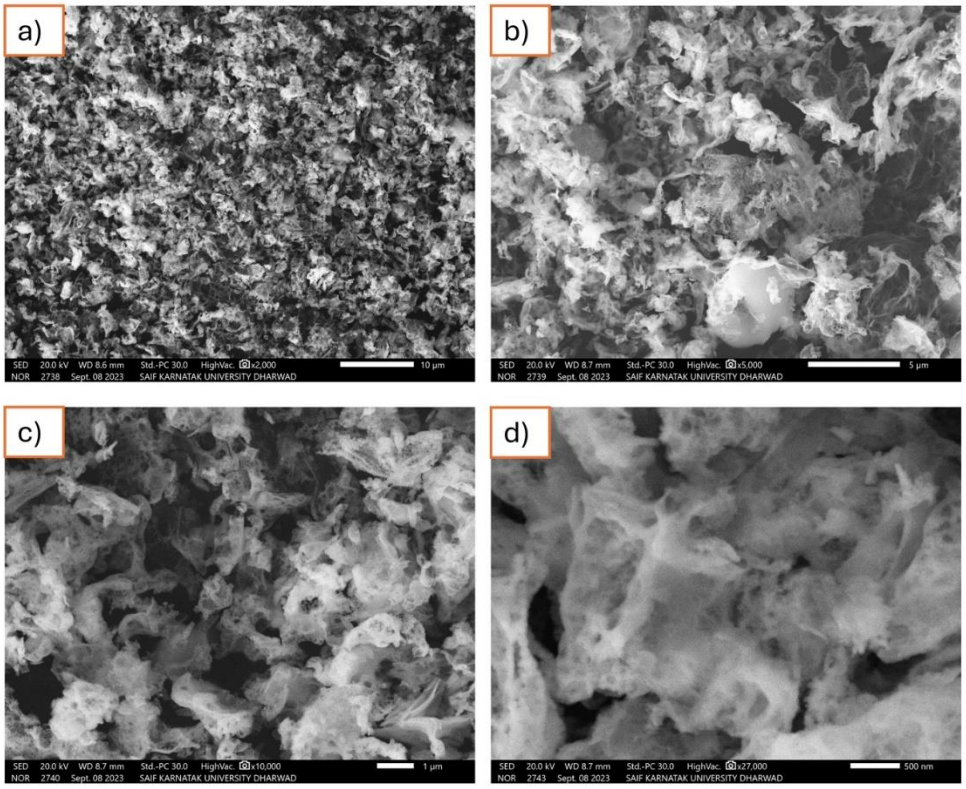

Figure 4. SEM images of WS-Ceria-NPs captured at progressive magnifications: **(a)** 10 µm scale reveals the overall morphology and spatial distribution; **(b)** 5 µm scale provides a closer view of particle clustering and surface texture; **(c)** 1 µm scale displays finer details of individual nanoparticles; **(d)** 500 nm scale highlights high-resolution nanoscale features and porosity.

3.5. EDX analysis.

The Energy Dispersive X-ray Spectroscopy (EDS) analysis confirmed the elemental composition of WS-Ceria-NPs, with cerium (Ce) and oxygen (O) as the primary components, validating the successful synthesis of ceria nanoparticles. The mass percentage of cerium was 49.77%, while oxygen accounted for 26.84%, aligning with the expected stoichiometry of CeO_2. Trace amounts of carbon, potassium, sodium, sulfur, chlorine, and aluminum were also detected, likely originating from the *W. somnifera* extract and synthesis process. Notably, the findings are consistent with those of Jannatul Mim *et al*., who reported the highest peaks for cerium at 4.8 keV and oxygen at 0.45 keV, perfectly aligning with the current study [54]. These elements, identified through K-shell (C, O, Na, S, Cl, K) and L-shell (Ce) X-ray transitions, are present in smaller quantities, with carbon contributing 13.52% to the overall mass, potentially due to residual organic compounds. Mamatha *et al*. also demonstrated the same X-ray transitions for cerium and oxygen in their study, further corroborating these findings [55]. The atom percentage of cerium (10.30%) supports the presence of Ce^{3+} and Ce^{4+} states, characteristic of cerium oxide. A detailed representation of the elemental composition is shown in Figure 3a, which illustrates the mass and atom percentages of each element analyzed. The porous, segregated nature of the nanoparticles, combined with their elemental composition, underscores the efficiency of the green synthesis method.

3.6. XRD analysis.

The X-ray Diffraction (XRD) analysis of the synthesized Ceria-NPs revealed a cubic fluorite structure, with prominent peaks at 2θ values of 28.44°, 33.01°, 47.40°, and 56.26°,

corresponding to the (111), (200), (220), and (311) planes of CeO_2, respectively, in accordance with standard JCPDS card numbers 00-067-0123 and 01-075-7752. Additional peaks at 58.98° (222), 69.35° (400), and 88.34° (422) further supported the crystalline structure (Figure 3b). These (hkl) values and their corresponding peaks perfectly align with the findings of Vettumperumal *et al*., reinforcing the reliability of the obtained data and confirming the characteristic cubic fluorite structure of Ceria-NPs [56]. Minor unidentified peaks, such as at 40.43° and 41.09°, suggest possible impurities or secondary phases. The average crystallite size of 43.7 nm (range: 32.8–60.1 nm) aligns closely with the 41 nm reported by Fatemeh Ghanbary and Ehsan Jafarnejad, validating the synthesis method [57]. The intensity distribution showed preferential growth along the (111) and (200) planes, indicative of the thermodynamic stability of the CeO_2 structure. These findings demonstrate the successful synthesis of high-quality CeO_2 nanoparticles, suitable for catalysis, biomedical applications, and environmental remediation, owing to their crystalline stability, nanocrystalline size, and enhanced surface area.

3.7. Zeta potential analysis.

The zeta potential of the WS-Ceria-NPs was recorded as -40.9 mV, indicating strong surface charge and excellent colloidal stability (Figure 5). A zeta potential value above ±30 mV is generally considered sufficient to ensure electrostatic repulsion between particles, preventing aggregation and promoting long-term dispersion stability [58]. A comparable study by Xiaohui Ju *et al*. reported a zeta potential of -48 mV for poly(acrylic acid)-coated Ceria-NPs [59], attributing the enhanced stability to the surface functionalization. Although our nanoparticles lack such polymeric coatings, their high negative zeta potential reflects similar stability characteristics, likely due to negatively charged functional groups introduced during synthesis. This stability makes the WS-Ceria-NPs well-suited for diverse applications, including biomedical and environmental fields, where dispersion stability is critical.

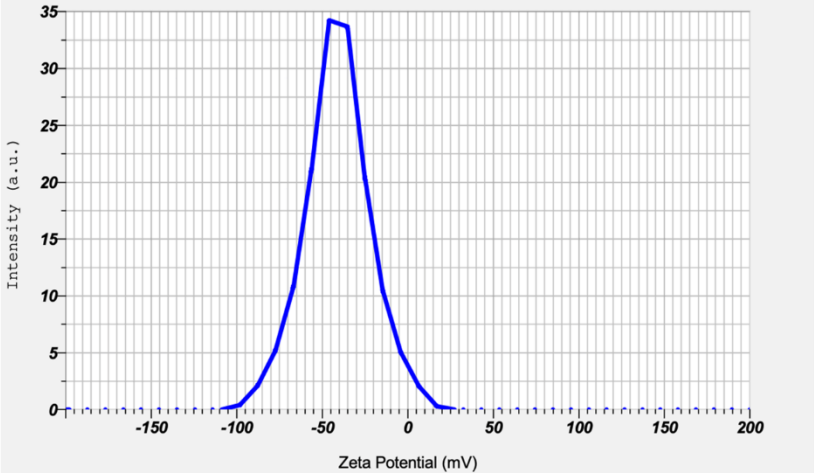

Figure 5. Zeta potential analysis of WS-Ceria-NPs showing a surface charge of –40.9 mV, indicative of strong electrostatic repulsion and excellent colloidal stability. This high negative potential reflects effective surface functionalization, which minimizes aggregation and enhances dispersion, making the nanoparticles suitable for biomedical applications.

3.8. TEM analysis.

The HRTEM analysis of the synthesized Ceria-NPs revealed a size distribution ranging from 9 to 26 nm, with the particles exhibiting a nearly oval shape (Figure 6a-b,g). Notably,

FFT analysis of the HRTEM images yielded a d-spacing of 0.32 nm, confirming the presence of a well-ordered crystalline lattice (Figure c-e). The Selected Area Electron Diffraction (SAED) pattern confirmed the crystalline nature of the nanoparticles, as evidenced by the distinct ring formation corresponding to various crystal planes (Figure 6f). Further analysis of the SAED pattern was performed using ImageJ software, where the radii of the diffraction rings were measured, and the corresponding d-spacing values were calculated. These values were compared with standard JCPDS data to identify the (hkl) planes. The observed (hkl) values, including (111), (200), (220), and (311), were consistent with the XRD results, confirming the cubic fluorite structure of the Ceria-NPs. Notably, a study by Eka Putri *et al*. reported a broader size range of 5–40 nm for Ceria-NPs based on TEM analysis, aligning with our findings [60]. Moreover, Aguiar De Oliveira *et al*. demonstrated that the (hkl) values obtained from XRD and SAED analyses matched, reinforcing the requirement that SAED results should correlate with XRD findings [61]. Similarly, our study also confirmed that the (hkl) values derived from SAED were in agreement with those obtained from XRD, further validating the structural integrity of the synthesized Ceria-NPs. This consistency highlights the reliability of SAED analysis in confirming crystallinity and phase identification. The crystalline morphology and nanoscale dimensions of the Ceria-NPs make them promising candidates for applications requiring high stability, such as catalysis and biomedical fields.

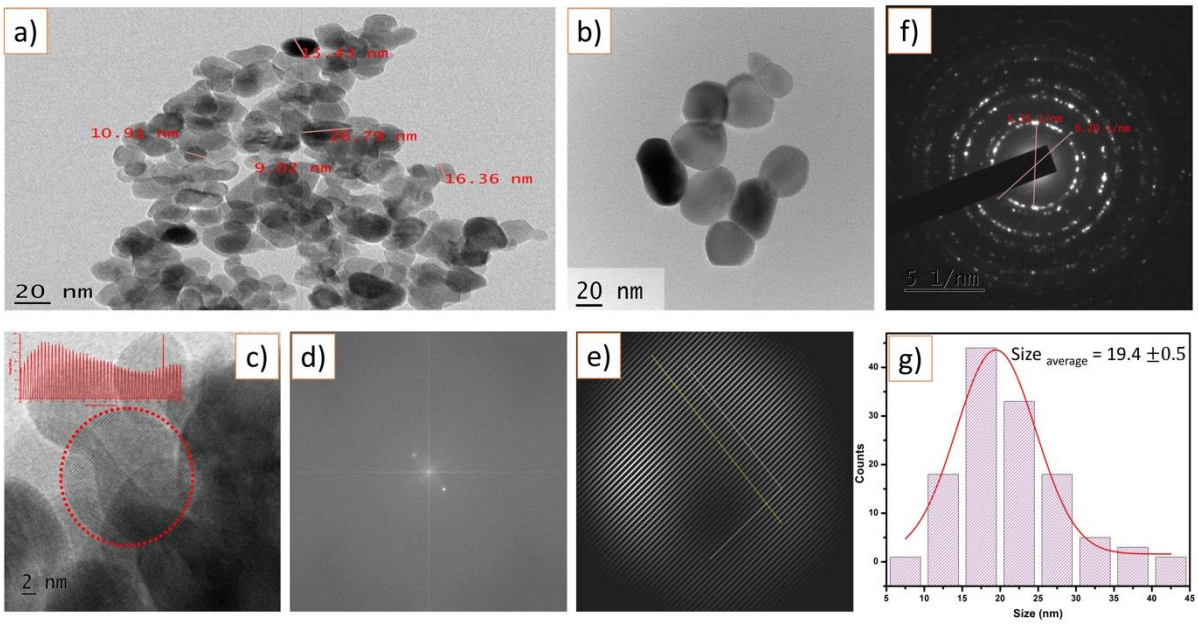

Figure 6. TEM analysis of WS-Ceria-NPs. **(a–c)** Transmission electron microscopy (TEM) images showing the nearly oval-shaped morphology of WS-Ceria-NPs with a size range of 9–26 nm; **(d–e)** Fast Fourier Transform (FFT) and inverse FFT analysis indicating a d-spacing of 0.32 nm, confirming the crystalline nature of the nanoparticles, with a yellow line drawn perpendicular to the plane highlighting lattice spacing; **(f)** Selected Area Electron Diffraction (SAED) pattern displaying distinct diffraction rings, validating the nanocrystalline structure; **(g)** Interplanar spacing analysis further supports the structural integrity of WS-Ceria-NPs.

3.9. Biocompatibility of ceria nanoparticles.

The biocompatibility of WS-Ceria-NPs was examined through antibacterial, antioxidant, anti-inflammatory, and nitric oxide inhibition assays, as detailed in the following subsections.

3.9.1. Antibacterial activity.

The antibacterial activity of ceria nanoparticles was assessed using the disc diffusion method on nutrient agar media against *Escherichia coli*. A single concentration of 100 µg of WS-Ceria-NPs was tested, with Ciprofloxacin as the standard antibiotic for comparison. After incubation, a clear zone of inhibition of approximately 18 mm was observed, demonstrating significant antibacterial potential (Figure 7). Dar *et al*. reported that as nanoparticle size decreases, antibacterial activity increases, which aligns with our findings [62,63]. The antibacterial mechanism of Ceria-NPs is primarily attributed to the generation of reactive oxygen species (ROS), which induce oxidative stress and cause structural damage to bacterial cells. Studies suggest that Ceria-NPs interact with lipids and proteins within the microbial membrane, disrupting its integrity and impairing essential cellular functions [64]. Additionally, the release of cerium ions from nanoparticle dissolution further inhibits microbial growth by interfering with nucleic acids, proteins, and polysaccharides, ultimately leading to bacterial death [65].

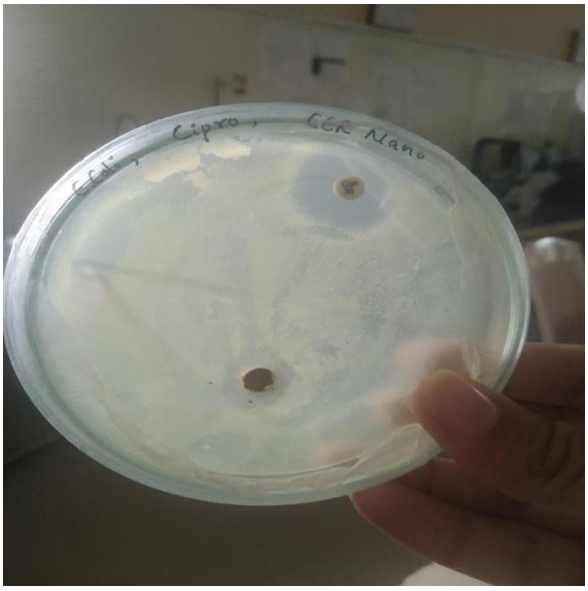

Figure 7. Antibacterial activity of WS-Ceria-NPs, exhibiting a clear zone of inhibition against *Escherichia coli* in a disc diffusion assay. The efficacy of the nanoparticles is compared to the standard antibiotic ciprofloxacin, underscoring their potential as effective antibacterial agents.

3.9.2. Minimum inhibitory concentration (MIC) determination.

The antibacterial activity of WS-Ceria-NPs was evaluated using the broth microdilution method to determine the MIC. Visual inspection of turbidity after 24 h of incubation at 37 °C showed that WS-Ceria-NPs at concentrations of 500, 250, 125, and 62.5 µg mL^{-1} completely inhibited bacterial growth, as no turbidity was observed, while the tube containing 31.25 µg mL^{-1} exhibited visible turbidity, indicating bacterial proliferation. These results, summarized in Table 1, establish the MIC of WS-Ceria-NPs against the tested bacterial strain as 62.5 µg mL^{-1}. The findings demonstrate a clear dose-dependent antibacterial effect of WS-Ceria-NPs. Complete inhibition of bacterial growth at concentrations ≥62.5 µg mL^{-1} suggests that the nanoparticles effectively interfere with bacterial viability, likely through mechanisms such as disruption of cell membranes and generation of reactive oxygen species [43]. Compared with the study by Pop *et al*., who reported an MIC of 2150 µg mL^{-1} for *E. coli*, the present results indicate that WS-Ceria-NPs exhibit strong antibacterial activity at lower concentrations, highlighting their potent efficacy [66]. The growth observed at 31.25 µg mL^{-1}

indicates that this concentration is below the threshold required to inhibit bacterial proliferation fully.

Table 1. MIC turbidity for different concentrations of WS-Ceria-NPs after 24h. Positive (+) turbidity indicates growth, and negative (-) no turbidity indicates the absence of growth.

Dilution of WS-Ceria-NPs	500 µg mL⁻¹	250 µg mL⁻¹	125 µg mL⁻¹	62.5 µg mL⁻¹	31.25 µg mL⁻¹
Set 1	–	–	–	–	+
Set 2	–	–	–	–	+
Set 3	–	–	–	–	+

3.9.3. Antioxidant activity.

The antioxidant activity of WS-Ceria-NPs was evaluated using the DPPH free radical scavenging assay, where the reduction in the violet DPPH radical was measured via UV-VIS spectroscopy. The scavenging activity increased with higher concentrations of WS-Ceria-NPs, with inhibition values of 42.86% and 19.24% at the high (250 µg mL^{-1}) and low (50 µg mL^{-1}) concentrations, respectively, compared to 32.95% and 13.68% for ascorbic acid (Figure 8). This dose-dependent increase in antioxidant activity indicates that WS-Ceria-NPs possess strong radical scavenging potential, likely due to their high surface area and reactivity, which are crucial for interacting with free radicals [67].

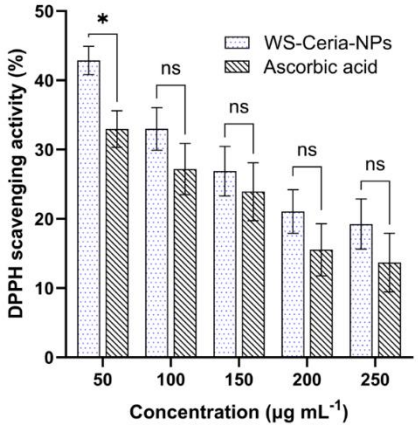

Figure 8. DPPH assay illustrating dose-dependent free radical scavenging activity, indicative of the WS-Ceria-NPs antioxidant potential. Bars represent mean ± SD ($^{ns}p > 0.05$, $*p < 0.05$, when compared with ascorbic acid).

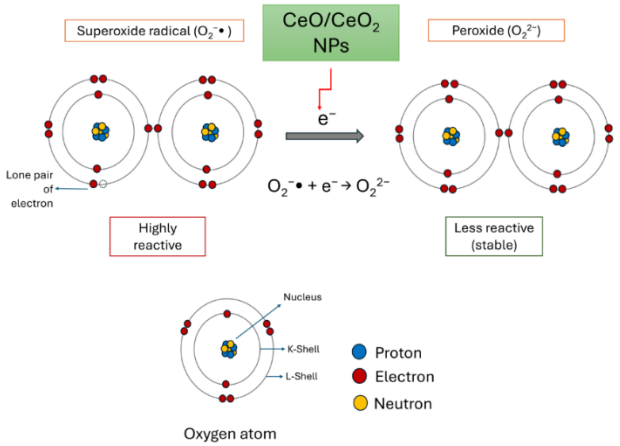

Figure 9. This figure illustrates the interaction between superoxide radicals (O_2^-) and cerium oxide nanoparticles (CeO/CeO_2 NPs). The superoxide radical, a highly reactive species, can accept an electron (e^-) to form a less reactive and more stable peroxide ion (O_2^{2-}). The cerium oxide nanoparticles play a crucial role in this electron transfer process, facilitating the conversion of the reactive superoxide radical into a more stable form. The diagram also highlights the presence of lone pairs of electrons and the fundamental particles (proton, electron, neutron) involved in these chemical interactions.

The higher activity observed at 250 µg mL^{-1} suggests that the WS-Ceria-NPs have a superior ability to neutralize DPPH radicals when compared to ascorbic acid, a standard antioxidant. The results support the potential of WS-Ceria-NPs as an effective antioxidant, which could be beneficial in biomedical applications, particularly in mitigating oxidative stress and related diseases. The possible mechanism is shown in Figure 9.

3.9.4. Anti-inflammatory activity.

The anti-inflammatory activity of WS-Ceria-NPs was assessed using the protein denaturation method, and the results demonstrated a concentration-dependent inhibition of protein denaturation. The WS-Ceria-NPs exhibited superior anti-inflammatory activity compared to the standard dexamethasone, with inhibition values of 55.56%, 51.74%, 42.01%, 29.86%, and 27.96% at concentrations of 50, 100, 150, 200, and 250 µg mL^{-1}, respectively, whereas the standard exhibited inhibition of 38.89%, 29.86%, 25%, 16.32%, and 11.11% at the same concentrations (Figure 10). These results indicate that WS-Ceria-NPs effectively prevent protein denaturation, a key process in inflammation.

The strong anti-inflammatory activity of WS-Ceria-NPs can be attributed to their unique nanozyme properties. As reported by Corsi *et al.*, ceria nanoparticles act as biomimetic nanozymes with superoxide dismutase (SOD)- and catalase-like activities, enabling them to scavenge reactive oxygen species (ROS) through a self-regenerating Ce^{3+}/Ce^{4+} redox cycle [68]. Since oxidative stress plays a pivotal role in inflammation, the ability of WS-Ceria-NPs to mitigate ROS levels could be a primary mechanism for their observed anti-inflammatory effects. Furthermore, ceria nanoparticles have been shown to modulate inflammatory pathways beyond ROS scavenging, including phosphatase activity, which could contribute to the inhibition of protein denaturation observed in this study.

Overall, the significant anti-inflammatory potential of WS-Ceria-NPs highlights their potential as a promising therapeutic agent for inflammatory conditions. Future studies focusing on molecular mechanisms and *in vivo* models would provide further insights into their clinical applicability.

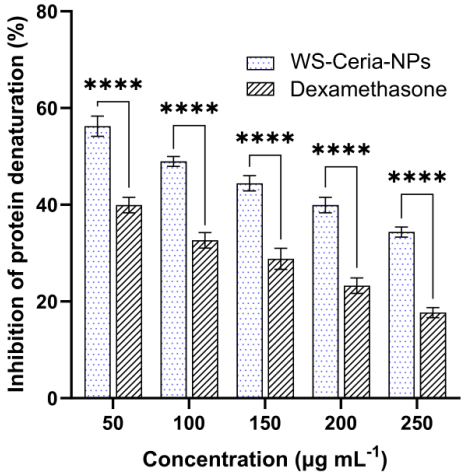

Figure 10. Protein denaturation inhibition assay demonstrating a concentration-dependent reduction in protein denaturation, reflective of significant anti-inflammatory effects by WS-Ceria-NPs. Bars represent mean ± SD (****$p < 0.0001$ when compared with dexamethasone).

3.9.5. NOX assay.

The nitric oxide (NO) assay demonstrated the potential of WS-Ceria-NPs in modulating NO production in colon cancer pancreatic cells. The LPS-treated group showed a significant

increase in NO levels (0.26), indicating an inflammatory response. However, treatment with WS-Ceria-NPs resulted in a concentration-dependent reduction in NO levels, with values of 0.20, 0.22, and 0.24 for 20 µL, 40 µL, and 60 µL of WS-Ceria-NPs, respectively, compared to 0.21 observed with the standard (Figure 11). This reduction suggests that WS-Ceria-NPs exhibit anti-inflammatory properties by mitigating LPS-induced NO production [69]. The ability of Ceria-NPs to regulate oxidative stress is primarily attributed to their redox cycling between Ce^{3+} and Ce^{4+}, which enables reactive oxygen and nitrogen species (RONS) scavenging [70]. This supports the potential therapeutic application of WS-Ceria-NPs for managing inflammation-related disorders [20].

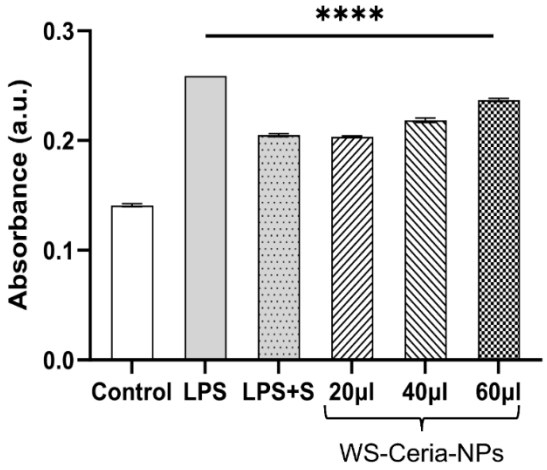

Figure 11. NOX assay showing the ability of WS-Ceria-NPs to modulate nitric oxide production in LPS-treated cells, further supporting their anti-inflammatory properties. Bars represent mean ± SD (****$p < 0.0001$ when compared with control).

4. Conclusions

This study demonstrates that *W. somnifera* leaf extract can be effectively utilized for the green synthesis of cerium oxide nanoparticles (WS-Ceria-NPs), providing an eco-friendly and sustainable alternative to conventional chemical methods. The innovation of this work lies in linking the plant's rich phytochemical composition to the formation of stable nanoparticles with unique dual band gap energies, enhancing their redox cycling between Ce^{3+} and Ce^{4+} states. This property underpins the observed multifunctional bioactivities, including potent antibacterial effects, strong free radical scavenging, and significant anti-inflammatory potential. Importantly, the NOX assay demonstrated that WS-Ceria-NPs regulate nitric oxide levels in LPS-treated cancer cells, highlighting their relevance to oxidative stress and inflammation-associated pathologies.

These findings underscore the importance of integrating medicinal plants into nanomaterial design to achieve multifunctional, biocompatible nanomaterials for biomedical use. Beyond their therapeutic promise, this approach offers a sustainable pathway to safer, scalable nanotechnology. Future work should focus on *in vivo* validation and mechanistic studies to translate WS-Ceria-NPs into clinically viable antimicrobial, antioxidant, and anti-inflammatory agents.

Author Contributions

Conceptualization, G.N. and S.M.B.; methodology, G.N., S.M.B., A.S., S.B. and S.G.; software, S.M.B., A.C.P. and B.T.; validation, R.B.Y. and B.R.L.; formal analysis, G.N., A.S.,

S.B., S.G. and S.R.S.; investigation, R.B.Y. and B.R.L.; resources, R.B.Y. and B.R.L.; data curation, S.M.B. and A.C.P.; writing—original draft preparation, S.M.B.; writing—review and editing, G.N., A.S., S.B., S.G., A.C.P., B.T., S.R.S., R.B.Y. and B.R.L.; visualization, G.N., A.S., S.B. and S.G.; supervision, R.B.Y. and B.R.L.; project administration, B.R.L. All authors have read and agreed to the published version of the manuscript.

Institutional Review Board Statement

Not applicable.

Informed Consent Statement

Not applicable.

Data Availability Statement

Data supporting the findings of this study are available from the corresponding author upon reasonable request.

Funding

The authors did not receive any specific grant from funding agencies in the public, commercial, or not-for-profit sectors.

Acknowledgments

The authors acknowledge the invaluable support of the Sophisticated Test and Instrumentation Center, Cochin University of Science and Technology, for their assistance with TEM analysis. Special thanks to the Sophisticated Analytical Instrument Facility, Dharwad, Karnatak University, and the DST PURSE Phase-II Program and University Scientific Instrumentation Center (USIC) of Karnatak University, Dharwad, for assistance with various analytical techniques. Additionally, we acknowledge Poornayu Research Labs, Nagarbhavi Extension, Bangalore, for some of the XRD and FTIR analysis. The authors also acknowledge the Laboratory of Natural Compound and Drug Discovery, Department of P. G. Studies and Research in Bioinformatics and Biotechnology, Vijayapura, Karnataka, India, and Department of Applied Genetics, Karnatak University, Dharwad, for the laboratory facility to carry out this research work.

Conflicts of Interest

The authors declare that there are no competing interests.

Abbreviations

The following abbreviations are used in this manuscript:

Abbreviation	Definition
WS-Ceria-NPs	*Withania somnifera*-derived Cerium Oxide Nanoparticles
ROS	Reactive Oxygen Species
RONS	Reactive Oxygen and Nitrogen Species
SOD	Superoxide Dismutase
DPPH	2,2-diphenyl-1-picrylhydrazyl
LPS	Lipopolysaccharide

Abbreviation	Definition
SAED	Selected Area Electron Diffraction
FFT	Fast Fourier Transform
HRTEM	High-Resolution Transmission Electron Microscopy
PBS	Phosphate-buffered Saline
BSA	Bovine Serum Albumin
NOX	Nitric Oxide Assay
XRD	X-ray Diffraction
SEM	Scanning Electron Microscopy
EDS/EDX	Energy Dispersive X-ray Spectroscopy
FTIR	Fourier Transform Infrared Spectroscopy
UV-Vis	Ultraviolet-visible Spectroscopy
SD	Standard Deviation
ANOVA	Analysis of Variance

References

1. Amani, A.M.; Vafa, E.; Mirzae, M.; Abbasi, M.; Vaez, A.; Najdian, A.; Jahanbin, A.; Kasaei, S.R.; Mosleh-Shirazi, S.; Kamyab, H. Mxenes as a versatile nanoplatform: synthesis and emerging biomedical applications. *J. Ind. Eng. Chem.* **2025**, *149*, 275-312, https://doi.org/10.1016/j.jiec.2025.02.020.
2. Zehra, S.H.; Ramzan, K.; Viskelis, J.; Viskelis, P.; Balciunaitiene, A. Advancements in Green Synthesis of Silver-Based Nanoparticles: Antimicrobial and Antifungal Properties in Various Films. *Nanomaterials* **2025**, *15*, 252, https://doi.org/10.3390/nano15040252.
3. Ma, X.; Tian, Y.; Yang, R.; Wang, H.; Allahou, L.W.; Chang, J.; Williams, G.; Knowles, J.C.; Poma, A. Nanotechnology in Healthcare, and Its Safety and Environmental Risks. *J. Nanobiotechnol.* **2024**, *22*, 715, https://doi.org/10.1186/s12951-024-02901-x.
4. Nagime, P.V.; Singh, S.; Chidrawar, V.R.; Rajput, A.; Syukri, D.M.; Marwan, N.T.; Shafi, S. Moringa Oleifera: A Plethora of Bioactive Reservoirs with Tremendous Opportunity for Green Synthesis of Silver Nanoparticles Enabled with Multifaceted Applications. *Nano-Struct. Nano-Objects***2024**, *40*, 101404, https://doi.org/10.1016/j.nanoso.2024.101404.
5. Bhavi, S.M.; Thokchom, B.; Singh, S.R.; Bajire, S.K.; Shastry, R.P.; Srinath, B.; Bhat, S.S.; Dupadahalli, K.; Govindasamy, C.; Chalekar, S.R. Syzygium malaccense leaf extract-mediated silver nanoparticles: synthesis, characterization, and biomedical evaluation in Caenorhabditis elegans and lung cancer cell line. *Green Chem. Lett. Rev.* **2025**, *18*, 2456624, https://doi.org/10.1080/17518253.2025.2456624.
6. Nagime, P.V.; Shaikh, N.M.; Shaikh, S.B.; Lokhande, C.D.; Patil, V.V.; Shafi, S.; Syukri, D.M.; Chidrawar, V.R.; Kumar, A.; Singh, S. Facile Synthesis of Silver Nanoparticles Using Calotropis Procera Leaves: Unraveling Biological and Electrochemical Potentials. *Discov. Nano* **2024**, *19*, 139, https://doi.org/10.1186/s11671-024-04090-w.
7. Nagime, P.V.; Singh, S.; Shaikh, N.M.; Gomare, K.S.; Chitme, H.; Abdel-Wahab, B.A.; Alqahtany, Y.S.; Khateeb, M.M.; Habeeb, M.S.; Bakir, M.B. Biogenic Fabrication of Silver Nanoparticles Using Calotropis Procera Flower Extract with Enhanced Biomimetics Attributes. *Materials* **2023**, *16*, 4058, https://doi.org/10.3390/ma16114058.
8. Milan, J.; Niemczyk, K.; Kus-Liśkiewicz, M. Treasure on the Earth—Gold Nanoparticles and Their Biomedical Applications. *Materials* **2022**, *15*, 3355, https://doi.org/10.3390/ma15093355.
9. Bhavi, S.M.; Raravi, L.M.; Medleri, R.H.; Padti, A.C.; Singh, S.R.; Thokchom, B.; Kulkarni, S.R.; Abbigeri, M.B.; Yarajarla, R.B. Microwave-Assisted Synthesis of Bio-Inspired Carbon Quantum Dots from Syzygium Malaccense Fruit: In-Vitro Anti-Diabetic Potential in 3T3-L1 Cell Line and Characterization. *Next Res.* **2025**, *2*, 100499, https://doi.org/10.1016/j.nexres.2025.100499.
10. Singh, S.R.; Bhavi, S.M.; Thokchom, B.; Abbigeri, M.B.; Padti, A.C.; Yadawad, A.; Harini, B.P.; Govindasamy, C.; Almutairi, K.M.; Yarajarla, R.B. An Evaluation of Carbon Dots Derived from Amaranthus Tricolor (L.) Leaves for Their Physicochemical, Photoluminescent, and Biomedical Properties. *Discov. Appl. Sci.* **2025**, *7*, 513, https://doi.org/10.1007/s42452-025-06936-z.
11. Hasan, M.; Altaf, M.; Zafar, A.; Hassan, S.G.; Ali, Z.; Mustafa, G.; Munawar, T.; Saif, M.S.; Tariq, T.; Iqbal, F. Bioinspired synthesis of zinc oxide nano-flowers: A surface enhanced antibacterial and harvesting efficiency. *Mater. Sci. Eng. C* **2021**, *119*, 111280, https://doi.org/10.1016/j.msec.2020.111280.
12. Saif, M.S.; Zafar, A.; Waqas, M.; Hassan, S.G.; Haq, A.U.; Tariq, T.; Batool, S.; Dilshad, M.; Hasan, M.; Shu, X. Phyto-Reflexive Zinc Oxide Nano-Flowers Synthesis: An Advanced Photocatalytic Degradation

and Infectious Therapy. *J. Mater. Res. Technol.* **2021**, *13*, 2375–2391, https://doi.org/10.1016/j.jmrt.2021.05.107.
13. Ramya, R.; Muthulakshmi, G.; Sudhahar, S.; Bhaskaran, A. Green Synthesis and Characterization Studies of TiO2 Nanoparticles and Its Potential Biological Performance. *Nano-Struct. Nano-Objects***2024**, *39*, 101322, https://doi.org/10.1016/j.nanoso.2024.101322.
14. Mundargi, N.N.; Sujatha, K.; B, S.R.; Dalbanjan, N.P.; S.K., P.K. Biogenic Copper Oxide Nanoparticles from *Chamaecostus Cuspidatus* Leaves: Dual Action Against Hyperglycemia and Oxidative Stress. *ChemistrySelect* **2025**, *10*, e01508, https://doi.org/10.1002/slct.202501508.
15. Bhavi, S.M.; Mirji, S.K.; Thokchom, B.; Singh, S.R.; Maliger, R.B.; Bhat, S.S.; Joshi, P.; Harini, B.; Yarajarla, R.B.; Jadidi, S.A. Potential Antidiabetic Properties of Syzygium Cumini (L.) Skeels Leaf Extract-Mediated Silver Nanoparticles. *Austin J. Anal. Pharm. Chem.* **2024**, *11*, 1168, https://doi.org/10.26420/austinjanalpharmchem.2024.1168.
16. Bhavi, S.M.; Padti, A.C.; Thokchom, B.; Singh, S.R.; Bhat, S.S.; Bajire, S.K.; Shastry, R.P.; Srinath, B.; Gummani, S.S.; Harini, B. Biogenic silver nanoparticles from Simarouba glauca DC leaf extract: Synthesis, characterization, and anticancer efficacy in lung cancer cells with protective effects in Caenorhabditis elegans. *Nano TransMed.* **2024**, *3*, 100052, https://doi.org/10.1016/j.ntm.2024.100052.
17. Padti, A.C.; Bhavi, S.M.; Thokchom, B.; Singh, S.R.; Bhat, S.S.; Harini, B.P.; Sillanpää, M.; Yarajarla, R.B. Nanoparticle Interactions with the Blood Brain Barrier: Insights from Drosophila and Implications for Human Astrocyte Targeted Therapies. *Neurochem. Res.* **2025**, *50*, 80, https://doi.org/10.1007/s11064-025-04333-x.
18. Hegde, S.; Balasubramanian, B.; Paul, R.; Jayalakshmi, M.; Nizam, A.; Pappuswamy, M.; Palani, V.; Kayamb, H.; Chelliapan, S.; Lakshmaiah, V.V. Navigating Green Synthesized Metal-Based Nanoparticles as Anti-Inflammatory Agent – Comprehensive Review. *Int. J. Pharm.* **2025**, *670*, 125105, https://doi.org/10.1016/j.ijpharm.2024.125105.
19. Nosrati, H.; Heydari, M.; Khodaei, M. Cerium Oxide Nanoparticles: Synthesis Methods and Applications in Wound Healing. *Materials Today Bio* **2023**, *23*, 100823, https://doi.org/10.1016/j.mtbio.2023.100823.
20. Yi, L.; Yu, L.; Chen, S.; Huang, D.; Yang, C.; Deng, H.; Hu, Y.; Wang, H.; Wen, Z.; Wang, Y. The regulatory mechanisms of cerium oxide nanoparticles in oxidative stress and emerging applications in refractory wound care. *Front. Pharmacol.* **2024**, *15*, 1439960, https://doi.org/10.3389/fphar.2024.1439960.
21. Nagime, P.V.; Pandey, V.K.; Rajpal, C.; Jayeoye, T.J.; Kumar, A.; Chidrawar, V.R.; Singh, S. Biogenic Selenium Nanoparticles: A Comprehensive Update on the Multifaceted Application, Stability, Biocompatibility, Risk, and Opportunity. *Zeitschrift für Naturforschung C* **2025**, *80*, 627-655, https://doi.org/10.1515/znc-2024-0176.
22. Balciunaitiene, A.; Zehra, S.H.; Liaudanskas, M.; Zvikas, V.; Viskelis, J.; Nuapia, Y.B.; Siukscius, A.; Singh, P.K.; Janulis, V.; Viskelis, P. Biosynthesis of Silver Nanoparticles via Medusomyces Gisevii Fermentation with Origanum Vulgare L. Extract: Antimicrobial Properties, Antioxidant Properties, and Phytochemical Analysis. *Molecules* **2025**, *30*, 1706, https://doi.org/10.3390/molecules30081706.
23. Amani, A.M. Tayebi, L.; Vafa, E.; Jahanbin, A.; Abbasi, M.; Vaez, A.; Kamyab, H.; Chelliapan, S. Innovation Applications of MXenes in Biomedicine. *Mater. Today Commun.* **2024**, *40*, 109929, https://doi.org/10.1016/j.mtcomm.2024.109929.
24. Nagime, P.V.; Shaikh, N.M.; Singh, S.; Chandak, V.S.; Chidrawar, V.R.; Nweye, E.P. Metallic Nanostructures: An Updated Review on Synthesis, Stability, Safety, and Applications with Tremendous Multifunctional Opportunities. *PNT* **2025**, *13*, https://doi.org/10.2174/0122117385358312250108180301.
25. Vinukonda, A.; Bolledla, N.; Jadi, R.K.; Chinthala, R.; Devadasu, V.R. Synthesis of Nanoparticles Using Advanced Techniques. *Next Nanotechnol.* **2025**, *8*, 100169, https://doi.org/10.1016/j.nxnano.2025.100169.
26. Nagime, P.V.; Chandak, V.S. A Comprehensive Review of Nanomaterials Synthesis: Physical, Chemical, and Biological Approaches and Emerging Challenges. *Biocatal. Agric. Biotechnol.* **2024**, *62*, 103458, https://doi.org/10.1016/j.bcab.2024.103458.
27. Kazemi, S.; Hosseingholian, A.; Gohari, S.D.; Feirahi, F.; Moammeri, F.; Mesbahian, G.; Moghaddam, Z.S.; Ren, Q. Recent Advances in Green Synthesized Nanoparticles: From Production to Application. *Materials Today Sustainability* **2023**, *24*, 100500, https://doi.org/10.1016/j.mtsust.2023.100500.
28. Hano, C.; Abbasi, B.H. Plant-Based Green Synthesis of Nanoparticles: Production, Characterization and Applications. *Biomolecules* **2021**, *12*, 31, https://doi.org/10.3390/biom12010031.
29. Mikulska, P.; Malinowska, M.; Ignacyk, M.; Szustowski, P.; Nowak, J.; Pesta, K.; Szeląg, M.; Szklanny, D.; Judasz, E.; Kaczmarek, G. Ashwagandha (Withania somnifera)—current research on the health-

promoting activities: a narrative review. *Pharmaceutics* **2023**, *15*, 1057, https://doi.org/10.3390/pharmaceutics15041057.
30. Ezez, D.; Mekonnen, N.; Tefera, M. Phytochemical Analysis of *Withania Somnifera* Leaf Extracts by GC-MS and Evaluating Antioxidants and Antibacterial Activities. *Int. J. Food Prop.* **2023**, *26*, 581–590, https://doi.org/10.1080/10942912.2023.2173229.
31. Hasan, M.; Zafar, A.; Shahzadi, I.; Luo, F.; Hassan, S.G.; Tariq, T.; Zehra, S.; Munawar, T.; Iqbal, F.; Shu, X. Fractionation of Biomolecules in Withania Coagulans Extract for Bioreductive Nanoparticle Synthesis, Antifungal and Biofilm Activity. *Molecules* **2020**, *25*, 3478, https://doi.org/10.3390/molecules25153478.
32. Qasim, S.; Zafar, A.; Saif, M.S.; Ali, Z.; Nazar, M.; Waqas, M.; Haq, A.U.; Tariq, T.; Hassan, S.G.; Iqbal, F. Green synthesis of iron oxide nanorods using Withania coagulans extract improved photocatalytic degradation and antimicrobial activity. *J. Photochem. Photobiol. B, Biol.* **2020**, *204*, 111784, https://doi.org/10.1016/j.jphotobiol.2020.111784.
33. Chatzimentor, I.; Tsamesidis, I.; Ioannou, M.-E.; Pouroutzidou, G.K.; Beketova, A.; Giourieva, V.; Papi, R.; Kontonasaki, E. Study of Biological Behavior and Antimicrobial Properties of Cerium Oxide Nanoparticles. *Pharmaceutics* **2023**, *15*, 2509, https://doi.org/10.3390/pharmaceutics15102509.
34. Muteeb, G.; Rehman, M.T.; Shahwan, M.; Aatif, M. Origin of Antibiotics and Antibiotic Resistance, and Their Impacts on Drug Development: A Narrative Review. *Pharmaceuticals* **2023**, *16*, 1615, https://doi.org/10.3390/ph16111615.
35. Zamani, K.; Allah-Bakhshi, N.; Akhavan, F.; Yousefi, M.; Golmoradi, R.; Ramezani, M.; Bach, H.; Razavi, S.; Irajian, G.-R.; Gerami, M. Antibacterial effect of cerium oxide nanoparticle against Pseudomonas aeruginosa. *BMC Biotechnol.* **2021**, *21*, 68, https://doi.org/10.1186/s12896-021-00727-1.
36. Olufunmilayo, E.O.; Gerke-Duncan, M.B.; Holsinger, R.M.D. Oxidative Stress and Antioxidants in Neurodegenerative Disorders. *Antioxidants* **2023**, *12*, 517, https://doi.org/10.3390/antiox12020517.
37. Jomova, K.; Raptova, R.; Alomar, S.Y.; Alwasel, S.H.; Nepovimova, E.; Kuca, K.; Valko, M. Reactive Oxygen Species, Toxicity, Oxidative Stress, and Antioxidants: Chronic Diseases and Aging. *Arch Toxicol.* **2023**, *97*, 2499–2574, https://doi.org/10.1007/s00204-023-03562-9.
38. Chaudhary, P.; Janmeda, P.; Docea, A.O.; Yeskaliyeva, B.; Abdull Razis, A.F.; Modu, B.; Calina, D.; Sharifi-Rad, J. Oxidative Stress, Free Radicals and Antioxidants: Potential Crosstalk in the Pathophysiology of Human Diseases. *Front. Chem.* **2023**, *11*, 1158198, https://doi.org/10.3389/fchem.2023.1158198.
39. Siposova, K.; Huntosova, V.; Garcarova, I.; Shlapa, Y.; Timashkov, I.; Belous, A.; Musatov, A. Dual-Functional Antioxidant and Antiamyloid Cerium Oxide Nanoparticles Fabricated by Controlled Synthesis in Water-Alcohol Solutions. *Biomedicines* **2022**, *10*, 942, https://doi.org/10.3390/biomedicines10050942.
40. Chavda, V.P.; Feehan, J.; Apostolopoulos, V. Inflammation: The Cause of All Diseases. *Cells* **2024**, *13*, 1906, https://doi.org/10.3390/cells13221906.
41. Mitarotonda, R.; Giorgi, E.; Eufrasio-da-Silva, T.; Dolatshahi-Pirouz, A.; Mishra, Y.K.; Khademhosseini, A.; Desimone, M.F.; De Marzi, M.; Orive, G. Immunotherapeutic Nanoparticles: From Autoimmune Disease Control to the Development of Vaccines. *Biomater. Adv.* **2022**, *135*, 212726, https://doi.org/10.1016/j.bioadv.2022.212726.
42. Hkiri, K.; Elsayed Ahmed Mohamed, H.; Ghotekar, S.; Maaza, M. Green Synthesis of Cerium Oxide Nanoparticles Using Portulaca Oleracea Extract: Photocatalytic Activities. *Inorg. Chem. Commun.* **2024**, *162*, 112243, https://doi.org/10.1016/j.inoche.2024.112243.
43. Bhavi, S.M.; Thokchom, B.; Abbigeri, M.B.; Bhat, S.S.; Singh, S.R.; Joshi, P.; Yarajarla, R.B. Green Synthesis, Characterization, Antidiabetic, Antioxidant and Antibacterial Applications of Silver Nanoparticles from Syzygium Caryophyllatum (L.) Alston Leaves. *Process Biochem.* **2024**, *145*, 89–103, https://doi.org/10.1016/j.procbio.2024.06.017.
44. Medalia, A.; Byrne, B. Spectrophotometric Determination of of Cerium (IV). *Anal. Chem.* **1951**, *23*, 453–456, https://doi.org/10.1021/ac60051a017.
45. Heckert, E.G.; Karakoti, A.S.; Seal, S.; Self, W.T. The Role of Cerium Redox State in the SOD Mimetic Activity of Nanoceria. *Biomaterials* **2008**, *29*, 2705–2709, https://doi.org/10.1016/j.biomaterials.2008.03.014.
46. Chinnaiah, K.; Theivashanthi, T.; Kannan, K.; Revathy, M.S.; Maik, V.; Parangusan, H.; Jeyaseelan, S.C.; Gurushankar, K. Electrical and Electrochemical Characteristics of Withania Somnifera Leaf Extract Incorporation Sodium Alginate Polymer Film for Energy Storage Applications. *J. Inorg. Organomet. Polym.* **2022**, *32*, 583–595, https://doi.org/10.1007/s10904-021-02139-2.

47. Thill, A.S.; Lobato, F.O.; Vaz, M.O.; Fernandes, W.P.; Carvalho, V.E.; Soares, E.A.; Poletto, F.; Teixeira, S.R.; Bernardi, F. Shifting the Band Gap from UV to Visible Region in Cerium Oxide Nanoparticles. *Appl. Surf. Sci.* **2020**, *528*, 146860, https://doi.org/10.1016/j.apsusc.2020.146860.
48. Dubey, M.; Wadhwa, S.; Mathur, A.; Kumar, R. Progress in Mesoporous Ceria: A Review on Synthesis Strategies and Catalytic Applications. *Appl. Surf. Sci. Advances* **2022**, *12*, 100340, https://doi.org/10.1016/j.apsadv.2022.100340.
49. Dai, F.; Zhuang, Q.; Huang, G.; Deng, H.; Zhang, X. Infrared Spectrum Characteristics and Quantification of OH Groups in Coal. *ACS Omega* **2023**, *8*, 17064–17076, https://doi.org/10.1021/acsomega.3c01336.
50. M. Subathra; M. Vellaisamy GREEN SYNTHESIS AND CHARACTERIZATION OF CERIUM OXIDE NANOPARTICLES USING Piper Betle Leaves. *RJC* **2024**, *17*, 54–58, https://doi.org/10.31788/RJC.2024.1718325.
51. Tumkur, P.P.; Gunasekaran, N.K.; Lamani, B.R.; Nazario Bayon, N.; Prabhakaran, K.; Hall, J.C.; Ramesh, G.T. Cerium Oxide Nanoparticles: Synthesis and Characterization for Biosafe Applications. *Nanomanufacturing* **2021**, *1*, 176–189, https://doi.org/10.3390/nanomanufacturing1030013.
52. Monica Ahmad, N.; Aishah Hasan, N. Synthesis of Green Cerium Oxide Nanoparticles Using Plant Waste from Colocasia Esculenta for Seed Germination of Mung Bean (Vigna Radiata). *J. Nanotechnol.* **2023**, *2023*, 1–9, https://doi.org/10.1155/2023/9572025.
53. Pandya, T.; Patel, S.; Kulkarni, M.; Singh, Y.R.; Khodakiya, A.; Bhattacharya, S.; Prajapati, B.G. Zeolite-Based Nanoparticles Drug Delivery Systems in Modern Pharmaceutical Research and Environmental Remediation. *Heliyon* **2024**, *10*, e36417, https://doi.org/10.1016/j.heliyon.2024.e36417.
54. Mim, J.; Sultana, Mst.S.; Dhar, P.K.; Hasan, Md.K.; Dutta, S.K. Green Mediated Synthesis of Cerium Oxide Nanoparticles by Using *Oroxylum Indicum* for Evaluation of Catalytic and Biomedical Activity. *RSC Adv.* **2024**, *14*, 25409–25424, https://doi.org/10.1039/D4RA04132A.
55. Mamatha, M.G.; Ansari, M.A.; Begum, M.Y.; Prasad B, D.; Al Fatease, A.; Hani, U.; Alomary, M.N.; Sultana, S.; Punekar, S.M.; MB, N. Green synthesis of cerium oxide nanoparticles, characterization, and their neuroprotective effect on hydrogen peroxide-induced oxidative injury in human neuroblastoma (SH-SY5Y) cell line. *ACS Omega* **2024**, *9*, 2639-2649, https://doi.org/10.1021/acsomega.3c07505.
56. Vettumperumal, R.; Dhineshbabu, N.R.; Pv, E.; Kit, C.C. XRD Peak Profile and Inverse Pole Figure Analysis of Ceria (CeO2) Nanoparticles. *Iran J. Sci.* **2024**, *48*, 1653–1661, https://doi.org/10.1007/s40995-024-01710-z.
57. Ghanbary, F.; Jafarnejad, E. Removal of Malachite Green from the Aqueous Solutions Using Polyimide Nanocomposite Containing Cerium Oxide as Adsorbent. *Inorg. Nano-Met. Chem.* **2017**, *47*, 1675–1681, https://doi.org/10.1080/24701556.2017.1357598.
58. Singh, S.R.; Kittur, B.; Bhavi, S.M.; Thokchom, B.; Padti, A.C.; Bhat, S.S.; Bajire, S.K.; Shastry, R.P.; Srinath, B.; Sillanpää, M. The effect of Clitoria ternatea L. flowers-derived silver nanoparticles on A549 and L-132 human cell lines and their antibacterial efficacy in Caenorhabditis elegans *in vivo*. *Hybrid Adv.* **2025**, *8*, 100359, https://doi.org/10.1016/j.hybadv.2024.100359.
59. Ju, X.; Fučíková, A.; Šmíd, B.; Nováková, J.; Matolínová, I.; Matolín, V.; Janata, M.; Bělinová, T.; Hubálek Kalbáčová, M. Colloidal Stability and Catalytic Activity of Cerium Oxide Nanoparticles in Cell Culture Media. *RSC Adv.* **2020**, *10*, 39373–39384, https://doi.org/10.1039/D0RA08063B.
60. Eka Putri, G.; Rilda, Y.; Syukri, S.; Labanni, A.; Arief, S. Highly Antimicrobial Activity of Cerium Oxide Nanoparticles Synthesized Using Moringa Oleifera Leaf Extract by a Rapid Green Precipitation Method. *J. Mater. Res. Technol.* **2021**, *15*, 2355–2364, https://doi.org/10.1016/j.jmrt.2021.09.075.
61. Aguiar De Oliveira, L.V.; Checca Huaman, N.R.; Monteiro, S.N.; Costa, U.O.; Vitorazi, L. Characterization and Optimization of Cerium Oxide Nanoparticle-Doped Cellulose Acetate Films Using the Box-Behnken Design. *J. Mater. Res. Technol.* **2025**, *35*, 2736–2754, https://doi.org/10.1016/j.jmrt.2025.01.224.
62. Dar, M.A.; Gul, R.; Alfadda, A.A.; Karim, M.R.; Kim, D.W.; Cheung, C.L.; Almajid, A.A.; Alharthi, N.H.; Pulakat, L. Size-Dependent Effect of Nanoceria on Their Antibacterial Activity Towards *Escherichia Coli*. *Sci. Adv. Mater.* **2017**, *9*, 1248–1253, https://doi.org/10.1166/sam.2017.3098.
63. Dar, M.; Gul, R.; Karuppiah, P.; Al-Dhabi, N.; Alfadda, A. Antibacterial Activity of Cerium Oxide Nanoparticles against ESKAPE Pathogens. *Crystals* **2022**, *12*, 179, https://doi.org/10.3390/cryst12020179.
64. Hirst, S.M.; Karakoti, A.S.; Tyler, R.D.; Sriranganathan, N.; Seal, S.; Reilly, C.M. Anti-inflammatory Properties of Cerium Oxide Nanoparticles. *Small* **2009**, *5*, 2848–2856, https://doi.org/10.1002/smll.200901048.

65. Chen, S.; Wang, Y.; Bao, S.; Yao, L.; Fu, X.; Yu, Y.; Lyu, H.; Pang, H.; Guo, S.; Zhang, H. Cerium oxide nanoparticles in wound care: a review of mechanisms and therapeutic applications. *Front. Bioeng. Biotechnol.* **2024**, *12*, 1404651, https://doi.org/10.3389/fbioe.2024.1404651.
66. Pop, O.L.; Mesaros, A.; Vodnar, D.C.; Suharoschi, R.; Tăbăran, F.; Magerușan, L.; Tódor, I.S.; Diaconeasa, Z.; Balint, A.; Ciontea, L. Cerium oxide nanoparticles and their efficient antibacterial application in vitro against gram-positive and gram-negative pathogens. *Nanomaterials* **2020**, *10*, 1614, https://doi.org/10.3390/nano10081614.
67. Rahman, Md.M.; Islam, Md.B.; Biswas, M.; Khurshid Alam, A.H.M. In Vitro Antioxidant and Free Radical Scavenging Activity of Different Parts of Tabebuia Pallida Growing in Bangladesh. *BMC Res. Notes* **2015**, *8*, 621, https://doi.org/10.1186/s13104-015-1618-6.
68. Corsi, F.; Deidda Tarquini, G.; Urbani, M.; Bejarano, I.; Traversa, E.; Ghibelli, L. The Impressive Anti-Inflammatory Activity of Cerium Oxide Nanoparticles: More than Redox? *Nanomaterials* **2023**, *13*, 2803, https://doi.org/10.3390/nano13202803.
69. Brusini, R.; Varna, M.; Couvreur, P. Advanced Nanomedicines for the Treatment of Inflammatory Diseases. *Adv. Drug Deliv. Rev.* **2020**, *157*, 161–178, https://doi.org/10.1016/j.addr.2020.07.010.
70. Putri, G.E.; Labanni, A.; Arief, S.; Dafriani, P.; Darma, I.Y.; Handayani, S.; Widyastuti; Jaffar, N.; Mahmud, M.; Ritonga, A.H. Green Synthesis of Cerium Oxide Nanoparticles Using Citrus Nobilis Lour. Peel Extract and Evaluation of Their Potential as Antibacterial and Antioxidant Agents. *Case Stud. Chem. Environ. Eng.* **2025**, *11*, 101062, https://doi.org/10.1016/j.cscee.2024.101062.

Publisher's Note & Disclaimer